EUROPEAN ORGANISATION FOR NUCLEAR RESEARCH

CERN-PPE/90-187
December 14, 1990

# A DIRECT MEASUREMENT OF THE $Z^0$ INVISIBLE WIDTH BY SINGLE PHOTON COUNTING

The OPAL Collaboration

**Abstract**

The OPAL detector at LEP is used to measure the branching ratio of the $Z^0$ into invisible particles by measuring the cross section of single photon events in $e^+e^-$ collisions at centre-of-mass energies near the $Z^0$ resonance. In a data sample of 5.3 $pb^{-1}$, we observe 73 events with single photons depositing more than 1.5 GeV in the electromagnetic calorimeter, with an expected background of $8 \pm 2$ events not associated with invisible $Z^0$ decay. With this data we determine the $Z^0$ invisible width to be $0.50 \pm 0.07 \pm 0.03$ GeV, where the first error is statistical and the second systematic. This corresponds to $3.0 \pm 0.4 \pm 0.2$ light neutrino generations in the Standard Model.

Submitted to Zeit. Phys. C

# The OPAL Collaboration


M.Z. Akrawy[12], G. Alexander[22], J. Allison[15], P.P. Allport[5], K.J. Anderson[9], J.C. Armitage[6], G.T.J. Arnison[19], P. Ashton[15], G. Azuelos[17,d], J.T.M. Baines[15], A.H. Ball[16], J. Banks[15], G.J. Barker[12], R.J. Barlow[15], J.R. Batley[5], G. Beaudoin[17], A. Beck[22], J. Becker[10], T. Behnke[8], K.W. Bell[19], G. Bella[22], S. Bethke[11], O. Biebel[3], U. Binder[10], I.J. Bloodworth[1], P. Bock[11], H. Breuker[8], R.M. Brown[19], R. Brun[8], A. Buijs[8], H.J. Burckhart[8], P. Capiluppi[2], R.K. Carnegie[6], A.A. Carter[12], J.R. Carter[5], C.Y. Chang[16], D.G. Charlton[8], J.T.M. Chrin[15], P.E.L. Clarke[24], I. Cohen[22], W.J. Collins[5], J.E. Conboy[14], M. Couch[1], M. Coupland[13], M. Cuffiani[2], S. Dado[21], G.M. Dallavalle[2], S. De Jong[8], P. Debu[20], M.M. Deninno[2], A. Dieckmann[11], M. Dittmar[4], M.S. Dixit[7], E. Duchovni[25], I.P. Duerdoth[15], D.J.P. Dumas[6], P.A. Elcombe[5], P.G. Estabrooks[6], E. Etzion[22], F. Fabbri[2], P. Farthouat[20], H.M. Fischer[3], D.G. Fong[16], M.T. French[19], C. Fukunaga[23], A. Gaidot[20], O. Ganel[25], J.W. Gary[11], J. Gascon[17], N.I. Geddes[19], C.N.P. Gee[19], C. Geich-Gimbel[3], S.W. Gensler[9], F.X. Gentit[20], G. Giacomelli[2], V. Gibson[5], W.R. Gibson[12], J.D. Gillies[19], J. Goldberg[21], M.J. Goodrick[5], W. Gorn[4], D. Granite[21], E. Gross[25], J. Grunhaus[22], H. Hagedorn[10], J. Hagemann[8], M. Hansroul[8], C.K. Hargrove[7], I. Harrus[21], J. Hart[5], P.M. Hattersley[1], M. Hauschild[8], C.M. Hawkes[8], E. Heflin[4], R.J. Hemingway[6], R.D. Heuer[8], J.C. Hill[5], S.J. Hillier[1], D.A. Hinshaw[17], C. Ho[4], J.D. Hobbs[9], P.R. Hobson[24], D. Hochman[25], B. Holl[8], R.J. Homer[1], S.R. Hou[16], C.P. Howarth[14], R.E. Hughes-Jones[15], R. Humbert[10], P. Igo-Kemenes[11], H. Ihssen[11], D.C. Imrie[24], L. Janissen[6], A. Jawahery[16], P.W. Jeffreys[19], H. Jeremie[17], M. Jimack[8], M. Jobes[1], R.W.L. Jones[12], P. Jovanovic[1], D. Karlen[6], K. Kawagoe[23], T. Kawamoto[23], R.G. Kellogg[16], B.W. Kennedy[14], C. Kleinwort[8], D.E. Klem[18], G. Knop[3], T. Kobayashi[23], T.P. Kokott[3], L. Köpke[8], R. Kowalewski[6], H. Kreutzmann[3], J. Kroll[9], M. Kuwano[23], P. Kyberd[12], G.D. Lafferty[15], F. Lamarche[17], W.J. Larson[4], J.G. Layter[4], P. Le Du[20], P. Leblanc[17], A.M. Lee[16], M.H. Lehto[14], D. Lellouch[8], P. Lennert[11], C. Leroy[17], L. Lessard[17], S. Levegrün[3], L. Levinson[25], S.L. Lloyd[12], F.K. Loebinger[15], J.M. Lorah[16], B. Lorazo[17], M.J. Losty[7], J. Ludwig[10], J. Ma[4,b], A.A. Macbeth[15], M. Mannelli[8], S. Marcellini[2], G. Maringer[3], A.J. Martin[12], J.P. Martin[17], T. Mashimo[23], P. Mättig[3], U. Maur[3], T.J. McMahon[1], J.R. McNutt[24], F. Meijers[8], D. Menszner[11], F.S. Merritt[9], H. Mes[7], A. Michelini[8], R.P. Middleton[19], G. Mikenberg[25], J. Mildenberger[6], D.J. Miller[14], C. Milstene[22], M. Minowa[23], W. Mohr[10], C. Moisan[17], A. Montanari[2], T. Mori[23], M.W. Moss[15], P.G. Murphy[15], W.J. Murray[5], B. Nellen[3], H.H. Nguyen[9], M. Nozaki[23], A.J.P. O'Dowd[15], S.W. O'Neale[8,c], B.P. O'Neill[4], F.G. Oakham[7], F. Odorici[2], M. Ogg[6], H. Oh[4], M.J. Oreglia[9], S. Orito[23], J.P. Pansart[20], G.N. Patrick[19], S.J. Pawley[15], P. Pfister[10], J.E. Pilcher[9], J.L. Pinfold[25], D.E. Plane[8], B. Poli[2], A. Pouladdej[6], E. Prebys[8], T.W. Pritchard[12], H. Przysiezniak[17], G. Quast[8], M.W. Redmond[9], D.L. Rees[1], M. Regimbald[17], K. Riles[4], C.M. Roach[5], S.A. Robins[12], A. Rollnik[3], J.M. Roney[9], S. Rossberg[10], A.M. Rossi[2,a], P. Routenburg[6], K. Runge[10], O. Runolfsson[8], S. Sanghera[6], R.A. Sansum[19], M. Sasaki[23], B.J. Saunders[19], A.D. Schaile[10], O. Schaile[10], W. Schappert[6], P. Scharff-Hansen[8], S. Schreiber[3], J. Schwarz[10], A. Shapira[25], B.C. Shen[4], P. Sherwood[14], A. Simon[3], P. Singh[12], G.P. Siroli[2], A. Skuja[16], A.M. Smith[8], T.J. Smith[8], G.A. Snow[16], R.W. Springer[16], M. Sproston[19], K. Stephens[15], H.E. Stier[10], R. Stroehmer[11], D. Strom[9], H. Takeda[23], T. Takeshita[23], P. Taras[17], N.J. Thackray[1], T. Tsukamoto[23], M.F. Turner[5], G. Tysarczyk-Niemeyer[11], D. Van den plas[17], R. Van Kooten[8], G.J. VanDalen[4], G. Vasseur[20], C.J. Virtue[18], H. von der Schmitt[11], J. von Krogh[11], A. Wagner[11], C. Wahl[10], J.P. Walker[1], C.P. Ward[5], D.R. Ward[5], P.M. Watkins[1], A.T. Watson[1], N.K. Watson[1], M. Weber[11], S. Weisz[8], P.S. Wells[8], N. Wermes[11], M. Weymann[8], G.W. Wilson[20], J.A. Wilson[1], I. Wingerter[8], V-H. Winterer[10], N.C. Wood[14], S. Wotton[8], T.R. Wyatt[15], R. Yaari[25], Y. Yang[4,b], G. Yekutieli[25], T. Yoshida[23], W. Zeuner[8], G.T. Zorn[16].

[1]School of Physics and Space Research, University of Birmingham, Birmingham, B15 2TT, UK
[2]Dipartimento di Fisica dell' Università di Bologna and INFN, Bologna, 40126, Italy
[3]Physikalisches Institut, Universität Bonn, D-5300 Bonn 1, FRG
[4]Department of Physics, University of California, Riverside, CA 92521 USA
[5]Cavendish Laboratory, Cambridge, CB3 0HE, UK
[6]Carleton University, Dept of Physics, Colonel By Drive, Ottawa, Ontario K1S 5B6, Canada
[7]Centre for Research in Particle Physics, Carleton University, Ottawa, Ontario K1S 5B6, Canada
[8]CERN, European Organisation for Particle Physics, 1211 Geneva 23, Switzerland
[9]Enrico Fermi Institute and Department of Physics, University of Chicago, Chicago Illinois 60637, USA
[10]Fakultät für Physik, Albert Ludwigs Universität, D-7800 Freiburg, FRG
[11]Physikalisches Institut, Universität Heidelberg, Heidelberg, FRG
[12]Queen Mary and Westfield College, University of London, London, E1 4NS, UK
[13]Birkbeck College, London, WC1E 7HV, UK
[14]University College London, London, WC1E 6BT, UK
[15]Department of Physics, Schuster Laboratory, The University, Manchester, M13 9PL, UK
[16]Department of Physics and Astronomy, University of Maryland, College Park, Maryland 20742, USA
[17]Laboratoire de Physique Nucléaire, Université de Montréal, Montréal, Quebec, H3C 3J7, Canada
[18]National Research Council of Canada, Herzberg Institute of Astrophysics, Ottawa, Ontario K1A 0R6, Canada
[19]Rutherford Appleton Laboratory, Chilton, Didcot, Oxfordshire, OX11 0QX, UK
[20]DPhPE, CEN Saclay, F-91191 Gif-sur-Yvette, France
[21]Department of Physics, Technion-Israel Institute of Technology, Haifa 32000, Israel
[22]Department of Physics and Astronomy, Tel Aviv University, Tel Aviv 69978, Israel
[23]International Centre for Elementary Particle Physics and Dept of Physics, University of Tokyo, Tokyo 113, and Kobe University, Kobe 657, Japan
[24]Brunel University, Uxbridge, Middlesex, UB8 3PH UK
[25]Nuclear Physics Department, Weizmann Institute of Science, Rehovot, 76100, Israel

[a]Present address: Dipartimento di Fisica, Università della Calabria and INFN, 87036 Rende, Italy
[b]On leave from Harbin Institute of Technology, Harbin, China
[c]On leave from Birmingham University
[d]and TRIUMF, Vancouver, Canada

## Introduction

Electron-positron collisions at centre-of-mass energies near and above the $Z^0$ resonance provide an opportunity to determine the content of light matter which interacts only through the weak force. Such particles contribute to the $Z^0$ invisible width, $\Gamma_{inv}$, if their masses are less than $M_{Z^0}/2$. In the Standard Model[1] the invisible width is expected to be[2] $0.501^{+0.005}_{-0.004}$ GeV from the three neutrino species, where the central value corresponds to the $Z^0$ mass of[3] $91.17 \pm 0.02$ GeV and a top quark mass of 150 GeV. The range of this prediction results from a variation of the top quark mass between 50 and 230 GeV. Additional generations or a new type of weakly interacting neutral particle would lead to a larger invisible width. The $Z^0$ invisible width could also be reduced, for example by the presence of right-handed neutrinos which mix with their left-handed counterparts.[4] Precision measurements of $\Gamma_{inv}$ have been made so far by subtracting the observed widths into multihadrons and charged leptons from the total width.[3,5] Our most recent result[3] obtained this way is $0.476 \pm 0.025$ GeV. This method, however, assumes that all visible decays of the $Z^0$ are accounted for in the analyses of the charged leptons and multihadrons.

In this paper a complementary approach is applied, which directly measures the cross section for events where the $Z^0$ decays into invisible particles. The events are signaled by a photon arising from initial state radiation. Over a decade ago, several authors[6] suggested that events of this kind could be used to determine the number of light neutrino generations. The cross section for the process $e^+e^- \rightarrow \nu\bar{\nu}\gamma$ can be written as[7]

$$\frac{d^2\sigma}{dE_\gamma \, d\cos\theta_\gamma} = H(E_\gamma, cos\theta_\gamma, s)\, \sigma_0(s') \tag{1}$$

where $H$ is a radiator function for photons of energy $E_\gamma$ and polar angle $\theta_\gamma$, $s$ is the square of the centre-of-mass energy, and $\sigma_0(s')$ is the "reduced" cross section for the process $e^+e^- \rightarrow \nu\bar{\nu}$, in the new centre-of-mass system, given by $s' = s - 2E_\gamma\sqrt{s}$. In lowest order and by approximating the W contribution by a four-point interaction, $\sigma_0$ is given by[6,7]

$$\sigma_0(s) = \frac{G_F^2\, s}{12\pi}\left(2 + \frac{N_\nu(g_v^2+g_a^2)}{\left[1-s/M_Z^2\right]^2 + \Gamma_Z^2/M_Z^2} + \frac{2(g_v+g_a)\left[1-s/M_Z^2\right]}{\left[1-s/M_Z^2\right]^2 + \Gamma_Z^2/M_Z^2}\right). \tag{2}$$

The dominant term is proportional to the number of light neutrino generations $N_\nu$ and comes from the square of the amplitude for $Z^0$ production, shown in figure 1 a. The first term arises from the square of the W-exchange diagram, figure 1 b, and the last term is the W−Z interference; combined they affect the overall cross section by less than 5 % for centre-of-mass energies between the $Z^0$ mass and 10 GeV above.[7]

In the past few years several experiments have measured single photon cross sections at energies well below the $Z^0$ resonance.[8,9] Altogether they measured a total of 3.9 events above background whereas 6.8 were expected for three neutrino generations, which gives a combined limit of less than 4.8 light neutrino generations at 95 % confidence level.[9]

At collision energies well above the $Z^0$ mass, initial state photon radiation which brings the electron-positron centre-of-mass energy back down to the $Z^0$ resonance is strongly favoured. Hence it has been argued that at energies some 10 GeV above the $Z^0$ mass the single photons could be easily observed and would allow for a precise measurement

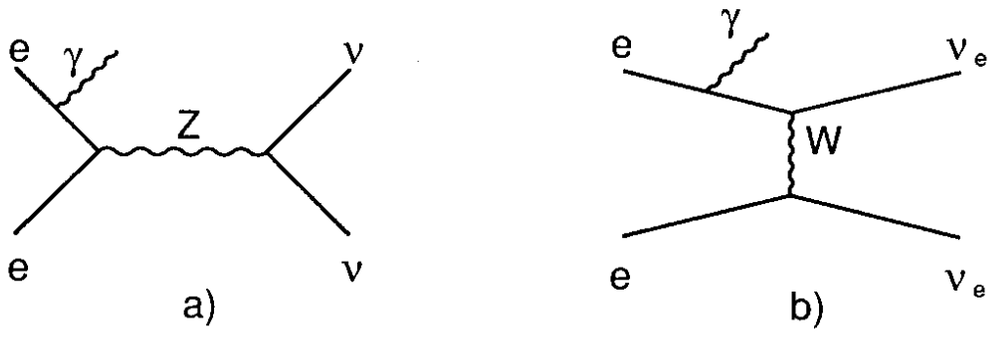


**Figure 1.** Two of the Feynman diagrams which contribute in lowest order to the process $e^+e^- \to \nu\bar{\nu}\gamma$. a) $Z^0$ decay allows the production of any of the light neutrino species. b) $W$ exchange produces only electron neutrinos.

of the invisible width.[6] The measurement described here uses data collected in 1990 with the OPAL detector at LEP at collision energies within only 3 GeV of the $Z^0$ resonance. Therefore events with low energy photons, near 1 GeV, must be used in the analysis. Such a measurement is more difficult than one using data at centre-of-mass energies far above the $Z^0$ peak for the following reasons: The detector must trigger efficiently on a small amount of energy, of order 1 % of the centre-of-mass energy, deposited in the electromagnetic calorimeter; potentially large backgrounds exist from processes in which some final state particles escape detection at angles close to the beam; the photon energy spectrum is falling rapidly and hence it is necessary to have a precise knowledge of the calorimeter energy scale.

To study the problems associated with the low energy single photon measurement, we use events with single electrons scattered at large angles as a high statistics control sample. These single electron events, which arise from the reactions $e^+e^- \to e^+e^-\gamma$ and $e^+e^- \to e^+e^-e^+e^-$, allow a determination of the trigger and event selection efficiencies, the background veto capability, and the calorimeter response to electromagnetic showers. Hence, both the single photon and the single electron analyses are explained thoroughly.

## The OPAL detector

The OPAL detector is described in detail elsewhere.[10] Charged particle tracking is provided by the central detector, consisting of the vertex, jet, and z chambers. The vertex chamber contains 36 azimuthal sectors of 18 wires and the jet chamber 24 sectors of 159 wires, to measure the momenta of charged particles. The ionization measurement from the jet chamber is used to calculate the mean energy loss, $dE/dx$, of particles traversing the chamber gas; electrons lose on average 10 keV/cm. A particle travelling perpendicularly to the beam direction traverses 0.08 radiation lengths from the interaction point to the outer radius of the jet chamber. The central detector is contained inside a pressure vessel and a solenoidal coil, which introduce an additional 1.8 radiation lengths of material at normal incidence.

The electromagnetic calorimeter consists of barrel and endcap arrays of lead glass blocks which cover the solid angles $|\cos\theta| < 0.82$ and $0.81 < |\cos\theta| < 0.98$ respectively, where $\theta$ is the polar angle with respect to the beam axis, with no gaps in the azimuthal angle $\phi$. The barrel lead glass blocks, approximately $10 \times 10$ cm$^2$ in cross section and

over 24 radiation lengths in depth, are located at a radius of 2.46 m from the beam axis, outside the coil. They are arranged to point slightly away from the interaction point to prevent neutral particles from escaping detection through the gaps between the blocks. The endcap lead glass blocks are arranged with their axes parallel to the beam direction in two arrays 2 m away on either side of the interaction point and provide a total depth of typically 22 radiation lengths. Clusters are formed from one or more contiguous blocks which contain signals above the thresholds of 20 MeV and 50 MeV for the barrel and endcap respectively. In this analysis, endcap clusters are only used if they contain two or more blocks; all barrel clusters above 100 MeV are used. (The cluster energies which are used in this analysis refer to the energy deposited in the lead glass, uncorrected for any energy a particle may lose before it enters the calorimeter.) Just in front of the lead glass blocks are gas presampler detectors. The barrel presampler consists of two cylindrical layers of limited streamer mode tubes with wires running axially. Clusters are found using the signals from the wires and from cathode strips on both sides of each layer, oriented at 45° to the wire direction. Directly in front of the barrel presampler is a cylindrical layer of 160 time-of-flight (TOF) scintillation counters, parallel to the beam axis. The TOF system covers the region $|\cos\theta| < 0.82$.

The return yoke of the magnet surrounds the lead glass arrays and is instrumented to form the hadron calorimeter. The barrel hadron calorimeter consists of nine layers of limited streamer mode tubes interleaved with 10 cm thick iron slabs. This analysis uses the signals from aluminium cathode strips running parallel to the streamer tubes to identify the presence of muons. The endcap and poletip hadron calorimeters extend the coverage to within 8° of the beam axis. Barrel and endcap muon detectors complement the muon identification with four layers of chambers outside the hadron calorimeter. Muon segments, formed from clusters of signals from the strips of the hadron calorimeters and muon detectors, are used in this analysis to veto events due to cosmic ray and beam halo muons.

The two forward detectors, each consisting of calorimeters, proportional tube chambers, drift chambers and scintillators, provide a luminosity measurement by counting low angle Bhabha events. In this analysis, the calorimeters are also used to veto events with an electron or a second photon scattering above 2°. A small gap between the forward and lead glass calorimeters is filled by a lead-scintillator sandwich of seven radiation lengths.

For Monte Carlo studies, a detector simulation program[11] is used which includes a detailed description of the detector geometry and material as well as effects of detector resolutions and efficiencies. It produces output identical in format to that of the detector data acquisition system, such that the data can be processed by the same analysis chain as the real events.

## Trigger

Events with only a single photon in the barrel region are recorded if either of the following trigger conditions are satisfied:

(a) A cluster exists in the barrel electromagnetic calorimeter whose energy is above a threshold of approximately 3 GeV.

(b) A cluster exists in the barrel electromagnetic calorimeter whose energy is above a lower threshold of approximately 1 GeV and which matches in azimuth with a TOF counter which fired within 40 ns of the beam crossing.

Since approximately 80 % of photons with normal incidence on the coil convert before reaching the TOF counters, the TOF-calorimeter coincidence provides an efficient trigger for low energy single photons.

The threshold behaviour of these triggers is studied by using events with a single electron in the barrel region. In addition to trigger conditions (a) or (b), such events are also recorded if they satisfy either of the following:

(c) A track found by the trigger electronics matches in $\theta$ and $\phi$ with an electromagnetic cluster above approximately 1 GeV.

(d) A track and a TOF counter which fired match in $\phi$.

## Single electron analysis

Events with a single electron in the barrel region provide an excellent control sample to study the detector response to low energy particles. Such events are selected by requiring that only one track exist, its point of closest approach to the origin be less than 30 cm along either beam direction and less than 6 mm in the perpendicular plane, and its momentum transverse to the beam axis be greater than 1 GeV. There must be an electromagnetic cluster with at least 500 MeV of energy deposited within $|\cos\theta| < 0.7$ and within 200 mrad of the track direction. The event must not contain a second cluster above 300 MeV in the electromagnetic calorimeter, separated by more than 200 mrad from the primary cluster. Single muon events are removed by requiring the mean energy loss as measured in the jet chamber, $dE/dx$, to be greater than 9 keV/cm, which is 98 % efficient for the single electron events.

A total of 5980 events satisfy these criteria. The observed transverse momentum and angular distributions of the events are shown in figure 2 to be described by the lowest order Monte Carlo expectations from radiative Bhabha scattering[12] $e^+e^- \rightarrow e^+e^-\gamma$ and two photon production[13] of electron pairs $e^+e^- \rightarrow e^+e^-e^+e^-$.

Events satisfying the track-TOF trigger coincidence (d) are used to determine the efficiency of the calorimeter triggers and the results are shown in figure 3. The low threshold trigger is more than 98 % efficient for deposited energies above 1.3 GeV; the high energy trigger reaches this efficiency at 3 GeV. The TOF efficiency is found to be $97.7 \pm 0.2$ %, and has no strong dependence on angle or energy. The efficiency of the track trigger is found to be $96.9 \pm 0.2$ %. The overall trigger efficiency for this single electron sample, which includes events depositing energies above 0.5 GeV, is determined by using the redundancy of conditions (a–d) to be $99.2 \pm 0.1$ %.

To compare the observed number of single electron events with that expected from the lowest order calculations, systematic effects from the acceptance, efficiencies, and backgrounds are taken into account. A correction factor of $1.01 \pm 0.02$ is applied to the observed cross section to account for effects which may not be properly accounted for in the detector simulation. The error is dominated by uncertainties in the transverse momentum

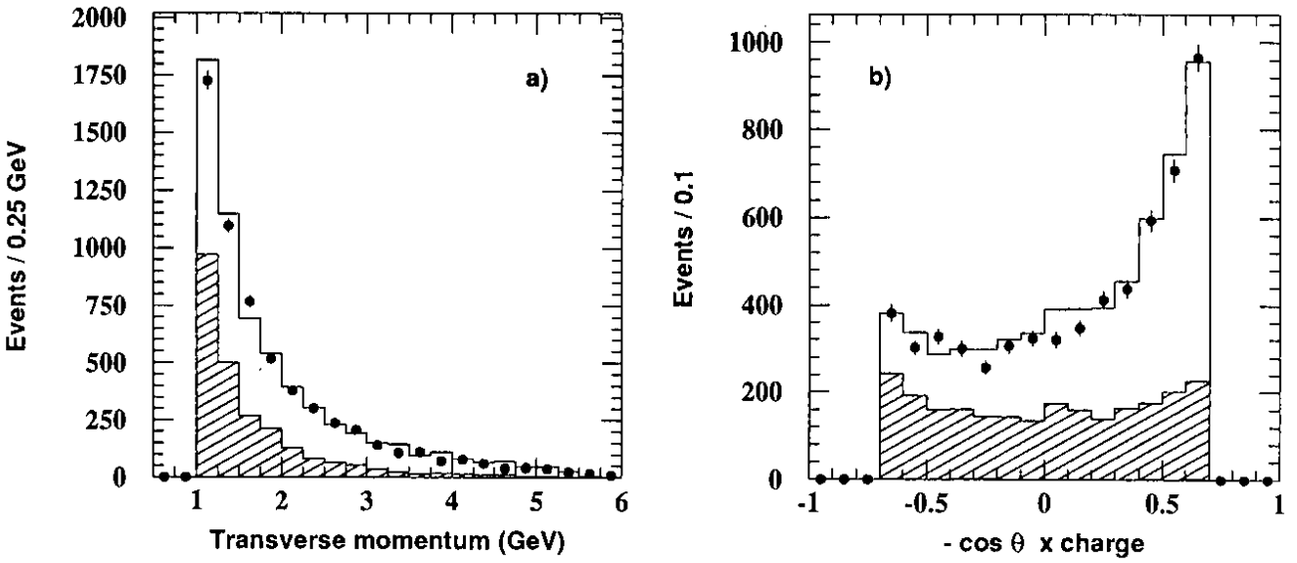


**Figure 2.** a) The observed transverse momentum spectrum and b) the angular distribution of single electron events compared with Monte Carlo expectations normalised to the integrated luminosity of 5.3 $pb^{-1}$. The shaded histograms show the contribution from the reaction $e^+e^- \rightarrow e^+e^-e^+e^-$, while the unshaded areas show the part from $e^+e^- \rightarrow e^+e^-\gamma$, with a strong asymmetry in the forward direction. The Monte Carlo statistics equal that of the data.

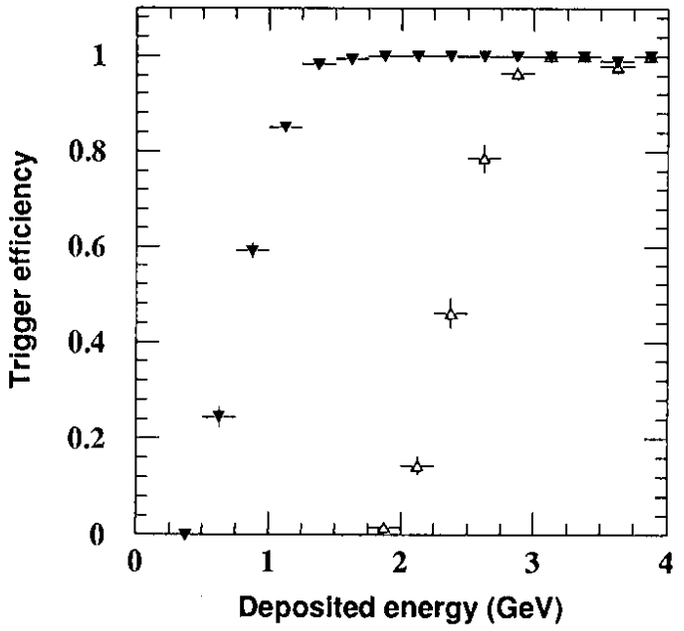


**Figure 3.** The efficiencies of the barrel electromagnetic calorimeter triggers are shown as determined from single electron events which trigger from a track-TOF coincidence. The solid triangles show the behaviour of the low threshold trigger which is used in coincidence with a track or TOF counter. The open triangles show the stand alone high threshold trigger.

measurement due to energy losses in the detector material. The background from two photon production of muon pairs is estimated from data and Monte Carlo simulation[13] to be $0.2 \pm 0.1$ %. After applying these corrections, the ratio of the observed cross section to

that expected from the lowest order Monte Carlo calculations is $0.96 \pm 0.01 \pm 0.02$, where the first error is statistical and the second systematic.

## Single photon analysis

Single photon candidates are selected by requiring the following:

(1) The deposited energy for a single photon, defined to be the total energy observed in a 200 mrad half-angle cone centred on the highest energy cluster in the region $|\cos\theta| < 0.7$, must be greater than 1 GeV. This highest energy cluster, combined with any clusters contiguous with it, must not extend more than 200 mrad in the polar or azimuthal directions, corresponding to more than five lead glass blocks in either direction. This requirement removes cosmic ray and beam halo muons which graze the barrel lead glass block array.

(2) No other cluster may be present more than 200 mrad away from this largest one anywhere in the barrel or endcap electromagnetic calorimeter with more than 300 MeV deposited energy.

(3) There must be no reconstructed central detector track with 20 or more jet chamber hits.

(4) To remove background from beam wall and beam gas interactions, the event must contain no vertex chamber sector with 5 or more hits and no jet chamber sector with 50 or more hits.

(5) The energy deposited in each forward calorimeter must be less than 2 GeV.

(6) To remove background from cosmic ray and beam halo events, at least one presampler cluster must exist within a 400 mrad half-angle cone around the photon direction, and the presampler cluster with the largest signal inside this cone must match the electromagnetic cluster coordinates to within 50 mrad.

(7) Remaining cosmic ray events are rejected if they contain a reconstructed muon segment in any of the hadron calorimeters or muon chambers, or strips with signals in three or more of the outer 8 layers of the barrel hadron calorimeter in any 45° azimuthal road. In addition, the number of strips hit in any of the hadron calorimeter barrel or endcap sectors must be less than 5.

There is a total of 136 events which satisfy these criteria. Since backgrounds are smaller and better understood for higher energy single photons, only the 73 events with single photons depositing more than 1.5 GeV in the calorimeter are used to determine the $Z^0$ invisible width. The events between 1 and 1.5 GeV are used as a background control sample, with which to verify the background estimates.

**Efficiency of the single photon selection**

The efficiency of the single photon selection is determined from a variety of data samples. The selection of the single electron sample is described above. A sample of tagged single photons from the processes $e^+e^- \to e^+e^-\gamma$ and $e^+e^- \to \gamma\gamma\gamma$ is selected by requiring the events satisfy all criteria except (5) and that they are tagged by more than half the beam energy being deposited in one forward calorimeter with less than 2 GeV in the other. Also used are events from $e^+e^- \to \gamma\gamma$[14] and $e^+e^- \to l^+l^-\gamma$, where $l$ is an electron or muon and both leptons are scattered at wide angles. Finally, 80287 random beam crossing events recorded throughout the data taking are used to measure inefficiencies introduced by sources of noise.

*Trigger efficiency*

The trigger efficiency is estimated using the threshold behaviour as measured with single electron events, as shown in figure 3, and by using the deposited energy spectrum from a Monte Carlo sample[15] of $e^+e^- \to \nu\bar{\nu}\gamma$ events which satisfy the single photon selection. For the complete sample of single photons which satisfy the selection criteria and deposit between 1 and 1.5 GeV in the electromagnetic calorimeter, the trigger efficiency is $89.2 \pm 3.1$ %; above 1.5 GeV this improves to $98.7 \pm 0.1$ %.

*Efficiency of the calorimeter requirements*

The cluster size limits of 200 mrad in the polar and azimuthal angle are satisfied by all 5980 single electron events except for one which has a photon radiated very near the electron direction.

The isolation requirement that no other cluster be present above 300 MeV is demonstrated in figure 4. The energy spectrum of clusters separated by more than 200 mrad from the highest energy barrel cluster for events which pass all criteria except for cut (2), is shown for the barrel and endcap calorimeters separately. Also shown is the occupancy measured in random beam crossing events. Below 300 MeV the additional clusters are consistent with random processes, whereas above 300 MeV there is a small excess. This excess is discussed in the section dealing with backgrounds from two photon production. The inefficiency of the isolation requirement due to random noise is determined from random beam crossings to be $0.5 \pm 0.1$ %. A Monte Carlo simulation[15], including the double radiative process $e^+e^- \to \nu\bar{\nu}\gamma\gamma$, indicates that if this requirement were removed, only 2.0 % additional events would be selected.

*Efficiency of the detector occupancy requirements*

Criteria (3) and (4) remove events with activity in the central detector, and hence single photons which convert in the beam pipe or in the volume of the central detector are excluded from the sample. The photon conversion probability in these regions is compared with the detector simulation by using events from the reaction $e^+e^- \to \gamma\gamma$. In the region $|\cos\theta| < 0.7$, $5.7 \pm 2.2$ % of the photons are observed to convert (as defined by failing cut (3)), in good agreement with the expectation of $5.9 \pm 0.7$ % from the simulation. A search is made for single photon events which convert in the central detector after passing

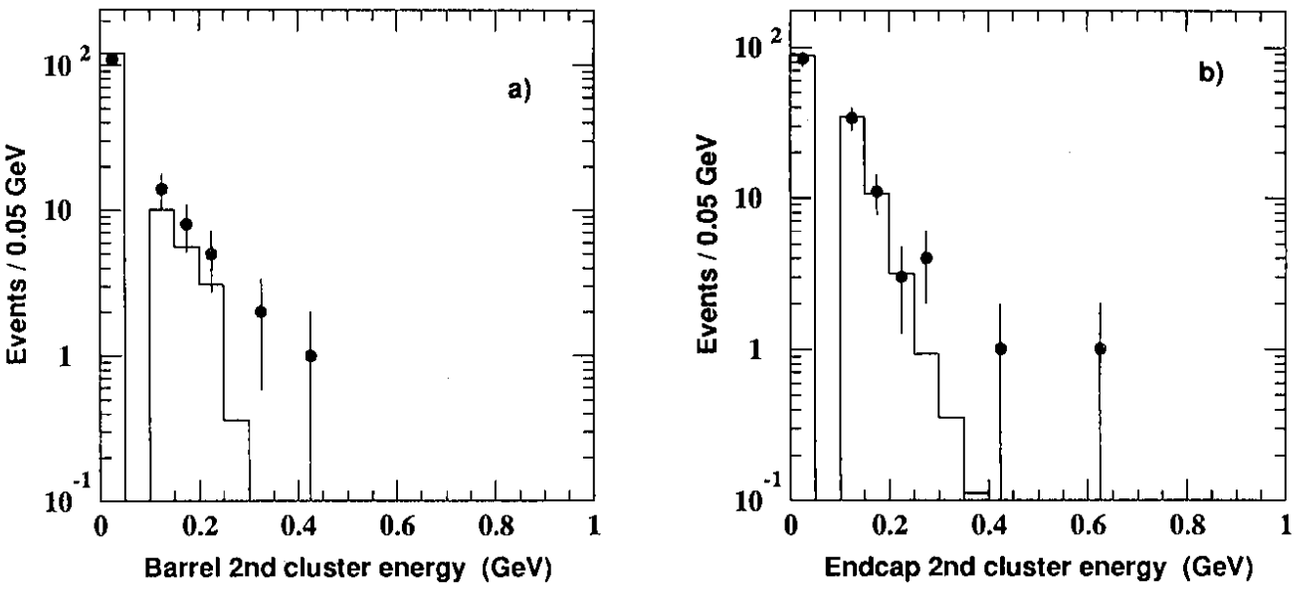


**Figure 4.** The spectra of the next highest energy cluster separated from the highest energy barrel cluster by more than 200 mrad are shown for single photon candidate events by the points for a) the barrel and b) the endcap electromagnetic calorimeter. The histograms show the spectra of cluster energies measured in random beam crossings, normalised to the number of single photon candidates. To pass the single photon selection, candidate events must not have a second cluster above 300 MeV. The first bin in each histogram shows the number of events with no other cluster above 100 MeV.

through the inner part of the vertex chamber by selecting events which would pass the single electron selection, except that two tracks are found within 30° in azimuth and fewer than 10 hits are found in the vertex chamber. Seven such events are observed compared to the Monte Carlo expectation of $4.6 \pm 1.0$ events. Overall, the estimated loss of $e^+e^- \to \nu\bar{\nu}\gamma$ events from the detector simulation of photon conversions in the beam pipe and central detector is $5.8 \pm 0.5$ %. To account for the uncertainty in the material in the central detector, this inefficiency is taken to be $6 \pm 2$ %. Apart from conversions, the inefficiency of the requirement that no central detector track be found in single photon events is negligible.

The inefficiency introduced by the muon rejection, cut (7), is observed to be $0.8 \pm 0.1$ % for the single electron sample, consistent with an estimate of $0.6 \pm 0.1$ % from random beam crossings. This indicates that the probability for a low energy electromagnetic shower to punch through to the hadron calorimeter is very small. The combined inefficiency of the occupancy requirements (2), (4), (5), and (7) is determined from random beam crossing events to be $2.5 \pm 0.1$ %.

*Efficiency of the presampler requirements*

The single photon selection requires a signal to be present in the presampler near the shower, and hence only those photons which convert in the material in front of the presampler are selected. Various samples of isolated photons are used to measure the photon conversion efficiency of the coil. Of the 87 tagged single photon events selected

**Table 1.** The efficiency of the presampler requirements is studied with a variety of data samples. Shown are the coil conversion probability and the efficiency for the presampler matching for both the data and Monte Carlo simulations. The difference between the predicted conversion efficiencies for the three samples is expected to be due to the different angular distributions. From the level of agreement observed, a systematic uncertainty of 3% is assigned to the simulation of the coil conversion, and 2% for the simulation of the matching requirement.

| Coil conversion (%) | data | Monte Carlo |
|---|---|---|
| tagged single photon events | $75.9 \pm 4.6$ | $84.2 \pm 2.4$ |
| $e^+e^- \to \gamma\gamma$ | $92.9 \pm 1.9$ | $88.5 \pm 1.7$ |
| $e^+e^- \to l^+l^-\gamma$ | $76.4 \pm 3.4$ | $80.9 \pm 1.3$ |

| Presampler match (%) | data | Monte Carlo |
|---|---|---|
| single electron events | $92.5 \pm 0.3$ | $95.4 \pm 0.3$ |
| tagged single photon events | $95.5 \pm 2.2$ | $96.0 \pm 1.1$ |

without the presampler requirement but which satisfy the high threshold calorimeter trigger (a), 66 events have a presampler cluster within 200 mrad of the shower or a TOF signal within 200 mrad in azimuth. This observed coil conversion efficiency of $75.9 \pm 4.6$ % is somewhat lower than the expected efficiency of $84.2 \pm 2.4$ % as estimated from the Monte Carlo detector simulation of tagged single photons from radiative Bhabha scattering[12], $e^+e^- \to e^+e^-\gamma$, and three photon production[16], $e^+e^- \to \gamma\gamma\gamma$. In the $e^+e^- \to \gamma\gamma$ sample, the observed conversion efficiency of $92.9 \pm 1.9$ % is slightly higher than the expectation of $88.5 \pm 1.7$ % from the detector simulation. In the radiative electron and muon pair events, $76.4 \pm 3.4$ % of photons are seen to convert, compared with the expectation of $80.9 \pm 1.3$ %. The comparisons between the measured and expected coil conversion efficiencies are summarised in table 1.

The Monte Carlo simulation of $e^+e^- \to \nu\bar{\nu}\gamma$ predicts that $82.1 \pm 1.3$ % of photons above 1 GeV convert in the coil. To allow for a possible error in the simulation, the efficiency for coil conversion is taken to be $82 \pm 3$ %.

By requiring the centroid of the presampler cluster with the largest signal to agree within 50 mrad of that found by the electromagnetic calorimeter, backgrounds from cosmic ray and beam halo muons are strongly suppressed. A presampler cluster exists for $97.1 \pm 0.2$ % of single electron events, and of these the fraction which satisfies the matching requirement is $95.3 \pm 0.3$ %, yielding an overall efficiency of $92.5 \pm 0.3$ %. The Monte Carlo simulation of single electron events has somewhat higher efficiencies; $97.6 \pm 0.2$ % and $97.7 \pm 0.2$ %, giving $95.4 \pm 0.3$ % overall. The efficiency shows no strong dependence on the energy or direction of the electron. The angular separation is shown in figure 5, for the single electrons, along with the single photon candidates, and suggests that the matching efficiency may be higher for photons than for electrons. To measure the matching efficiency for photons we use tagged single photon events which are selected without the presampler requirement but which have an in time TOF signal within 200 mrad in azimuth. Only one of the 89 events has no nearby presampler cluster and three others fail the matching requirement for an overall efficiency of $95.5 \pm 2.2$ %. This agrees with the Monte Carlo simulation of tagged single photon events which predicts an overall efficiency of $96.0 \pm 1.1$ %.

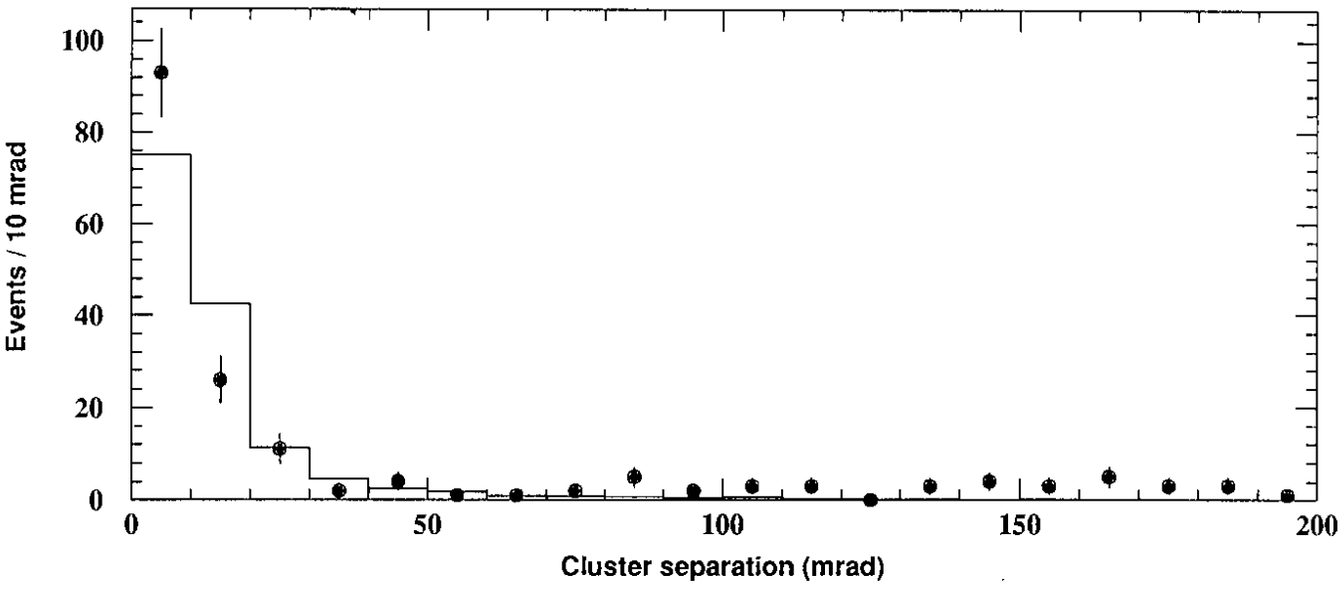


**Figure 5.** The separation between presampler and electromagnetic calorimeter clusters for single photon candidates is required to be less than 50 mrad. The points show this separation for candidate events passing all other cuts, and the histogram is the distribution from single electron events, normalised to the number of single photon candidates which survive this cut. Most of the events failing this cut alone originate from cosmic rays and beam halo.

In the Monte Carlo simulated sample of $e^+e^- \to \nu\bar{\nu}\gamma$ events, the efficiency for the presampler matching requirement is $96.9 \pm 0.4$ %. To account for a possible difference between the efficiencies for the data and Monte Carlo, the efficiency for this requirement is taken to be $97 \pm 2$ %.

*Check of the overall efficiency*

As an overall check of the analysis, the spectrum and angular distribution of the tagged single photon events are shown in figure 6 to agree with the expectation from the processes $e^+e^- \to e^+e^-\gamma$ and $e^+e^- \to \gamma\gamma\gamma$. After correcting for a trigger efficiency of $99.0 \pm 0.1$ % and for the efficiencies described above, the ratio of the observed cross section to that expected from the lowest order Monte Carlo calculations is $1.02 \pm 0.11 \pm 0.08$.

## Estimation of the background to single photons

*Radiative Bhabha scattering and $e^+e^-$ annihilation to three photons*

The dominant background to the $e^+e^- \to \nu\bar{\nu}\gamma$ process comes from low $Q^2$ radiative Bhabha scattering, in which both electrons escape at small angles with respect to the beam axis. It is shown in figure 6 that this process is understood when one electron scatters into the fiducial volume of the forward calorimeters. It is important therefore to verify the proper simulation of the region in which the forward calorimeters lose veto efficiency. Figure 7 shows the fraction of single electron events which deposit more than 2 GeV in either forward calorimeter, as a function of the transverse momentum of the wide angle

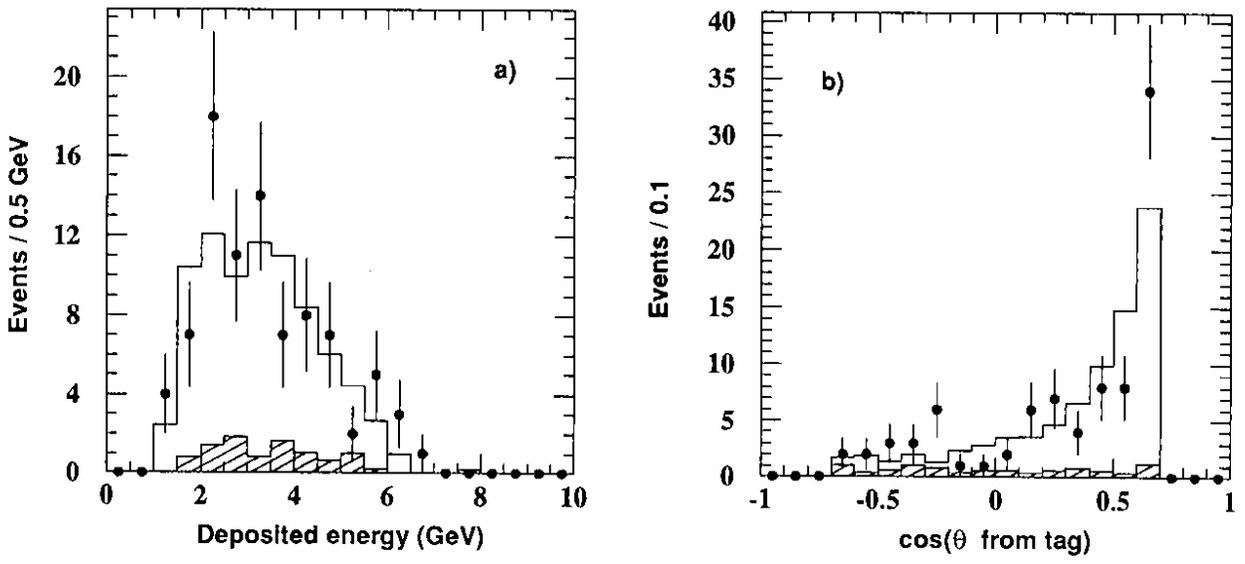


**Figure 6.** Single photon events, tagged by more than one half of the beam energy deposited in a forward calorimeter, are compared with the expectations from the reactions $e^+e^- \to e^+e^-\gamma$ (unshaded areas) and $e^+e^- \to \gamma\gamma\gamma$ (shaded histograms) and provide a check of the overall efficiency. Shown in a) is the spectrum of the single photons, and in b) the cosine of the angle between the photon and the beam axis from the tagging side. It is seen that the photons tend to be in the same $z$-hemisphere as the tag, as expected.

electron, compared with the Monte Carlo simulation. In the data, there are more tagged single electron events with transverse momentum below 1.5 GeV than expected from the lowest order calculations. For the lowest transverse momentum bin, excess events are observed over all polar angles of forward detector clusters with energies typically below half of the beam energy. We interpret the excess events in this bin to be coming from double radiative Bhabha scattering, $e^+e^- \to e^+e^-\gamma\gamma$. In the second bin of transverse momentum of figure 7, the excess events primarily have clusters at the inner edge of the forward calorimeters. In this case they are presumed to arise from an imprecise simulation near the inner edge, which can be accounted for by reducing the effective minimum veto angle by about 1 mrad. The Monte Carlo single photon background estimates are therefore reduced by $5 \pm 5$ % to account for the discrepancy in the tagging acceptance.

For the 1194 single electron events with transverse momentum above 2.5 GeV, the simulation predicts less than one event to deposit less than 2 GeV in either forward calorimeter, whereas eight are found; of these the highest transverse momentum is 5.4 GeV. Less than one event is expected to be the result of an asymmetric conversion of a photon from the process $e^+e^- \to \nu\bar{\nu}\gamma$. The additional contribution to the single photon background from $e^+e^- \to e^+e^-\gamma$ due to this apparent tagging inefficiency is less than 0.5 events for the complete data sample.

Overall, radiative Bhabha scattering is estimated from a Monte Carlo simulation[12] to contribute $13 \pm 2$ events to the single photon sample between 1 and 1.5 GeV in deposited energy, and $5 \pm 1$ events above 1.5 GeV.

The background from $e^+e^-$ annihilation into three photons, $e^+e^- \to \gamma\gamma\gamma$, is estimated

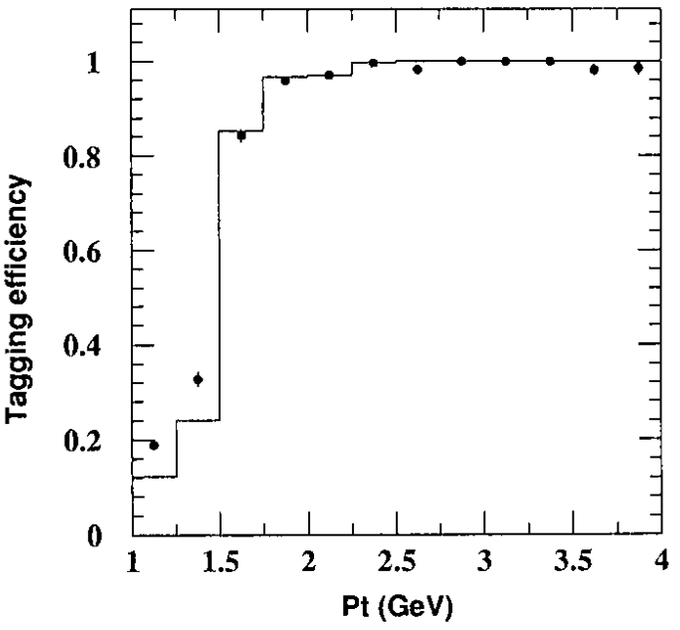


**Figure 7.** The fraction of single electron events depositing more than 2 GeV of energy in either forward calorimeter is shown as a function of the single electron transverse momentum for the data (points) and the Monte Carlo simulation (histogram).

by Monte Carlo simulation[16] to contribute $1 \pm 1$ events to the single photon sample between 1 and 1.5 GeV in deposited energy, and is negligible above 1.5 GeV.

*Two photon processes*

A potentially large background exists from two photon production of resonances, $e^+e^- \to e^+e^-X$, where $X$ is $f_2$, $\pi^0$, $\eta$, or $\eta'$.[7] The spectra of single photons from these sources are expected to be softer than that from radiative Bhabha scattering, and therefore these channels must be understood when studying very low energy single photons. Selection cut (2) removes multiphoton final states when a second photon deposits more than 300 MeV in the electromagnetic calorimeter. Monte Carlo samples of these events have been generated[17] in order to estimate their contribution to the single photon sample. In the data there is a total of five events which satisfy the single photon selection except that a second cluster exists with energy between 300 MeV and 1 GeV. This is comparable to the Monte Carlo expectation of $2.0 \pm 0.4$ from $e^+e^- \to \nu\bar{\nu}\gamma\gamma$, $3.3 \pm 1.3$ from two photon production of the $f_2$ and $1.6 \pm 0.2$ from random noise. A visual scan of the five events shows that two are consistent with two photon resonance production, one from radiative Bhabha scattering with an unreconstructed low angle electron, one from a cosmic ray event, and one is ambiguous. Between 1 and 1.5 GeV in deposited energy, the expected background from two photon production of resonances is $6 \pm 2$ events; with a 1.5 GeV threshold this reduces to $1 \pm 1$ event.

An accurate Monte Carlo event generator for the process $e^+e^- \to e^+e^-l^+l^-\gamma$ where $l$ is a lepton, is not available. One study[7] estimates that this background is negligible for single photons above 1.5 GeV, but could be as much as a third of the radiative Bhabha cross section for photons between 1 and 1.5 GeV. Hence we estimate that $4 \pm 4$ events contribute to the sample between 1 and 1.5 GeV, and neglect this background above 1.5 GeV.

*Other $Z^0$ decays*

The background from events in which the $Z^0$ decays into undetected charged particles, is evaluated by Monte Carlo simulation.[18] Only $\mu^+\mu^-\gamma$ final states are found to contribute a measurable background. In our data sample, this process is expected to contribute $0.6 \pm 0.4$ single photon events depositing between 1 and 1.5 GeV in the electromagnetic calorimeter, and $1.0 \pm 0.4$ events above 1.5 GeV. The cross section is largest above the $Z^0$ resonance. We take this background to contribute $1 \pm 1$ event in each single photon sample, below and above 1.5 GeV.

*Other backgrounds*

There can be large backgrounds which arise from cosmic rays, beam halo, beam wall and beam gas interactions. Their contribution to the single photon sample cannot be easily calculated. Instead, we estimate these backgrounds with the precise time measurement from the TOF system, which is not used in the event selection.

An estimate of the contamination of muons from cosmic rays and beam halo is possible by examining the TOF distribution of the single photon candidates. As shown in figure 8a, the differences between the measured and expected flight times are consistent with the TOF resolution, as demonstrated by the single electron events. From a visual scan, none of the four single photon candidates without TOF information has any evidence of activity from muons. Also shown in figure 8a is the distribution of events failing the single photon selection only by cut (6), and when the electromagnetic cluster size is allowed to be as large as 400 mrad in polar or azimuthal angles. The large number of events more than 6 ns early is due to beam halo muons which travel in time with the beam and cross the barrel electromagnetic calorimeter. No events of this type remain in the single photon sample. Since no single photon candidate has a measured time of flight more than 2 ns from the expected flight time, we assume that the cosmic ray and beam halo muons contribute no events to our sample.

Background events resulting from an interaction of a beam electron with the gas inside the LEP ring or with the beam pipe wall can generate photons from any point along the beam axis. Since such interactions will produce particles mainly in the forward direction, events generating photons in the barrel region will tend to originate upstream of the nominal collision point, and hence the particles will arrive at a TOF counter earlier than expected for a photon coming from an interaction at the origin. The measured time after the beam crossing, $t$, can thus be used to estimate the z coordinate of the interaction which produced the photon,

$$z_{\rm int} = \frac{t^2c^2 - R^2/\sin^2\theta}{2(tc - R|\cot\theta|)} \qquad (3)$$

where R is the distance from the beam axis to the TOF counters (R/c = 7.9 ns). With a TOF resolution of 250 ps observed for single electrons, the precision in the $z_{\rm int}$ measurement varies between 7.5 cm at $\cos\theta = 0$ and 25 cm at $|\cos\theta| = 0.7$ for photons coming from the interaction point. Figure 8b shows the distribution of $z_{\rm int}$ for the single electron and single photon events. Also shown are the 14 events which fail only requirement (4), that there be fewer than five hits in any vertex chamber sector and fewer than 50 in any jet chamber sector. These events were visually scanned; nine are consistent with beam gas or

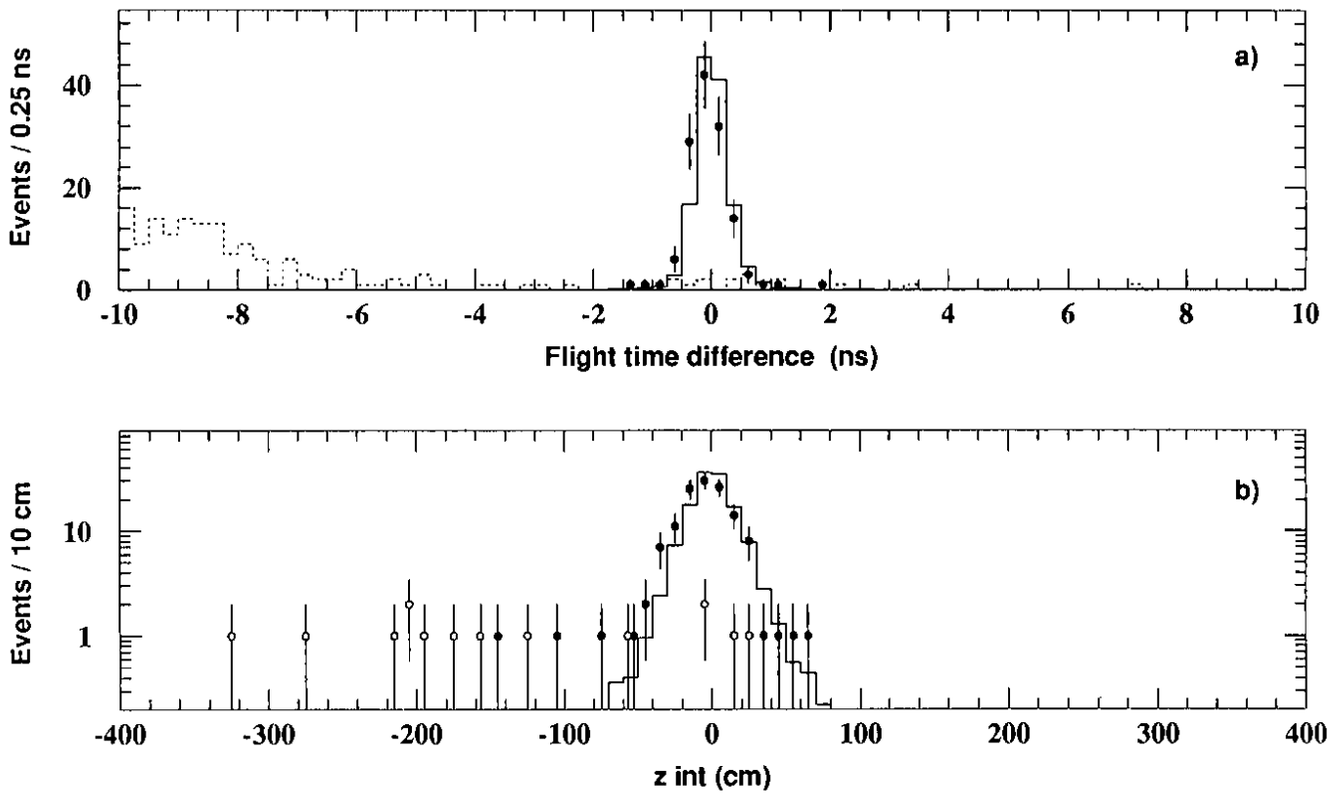


**Figure 8.** a) The measured minus expected flight times for single photon candidates (points) compared with the distribution from single electrons (solid histogram) and from events failing the presampler cluster requirement and when the electromagnetic cluster size is allowed to be as large as 400 mrad in polar or azimuthal angles (dashed histogram). b) The estimate, $z_{\rm int}$, of the $z$ coordinate of the interaction producing the photon, using the time of arrival at the TOF counters. Upstream production corresponds to $z_{\rm int} < 0$, which is expected for beam wall or beam gas production. The histogram is the distribution of the single electron sample, normalised to the single photon sample. The single photon candidates are indicated by the solid points. The open circles show beam gas - beam wall candidate events; those which fail the selection only by requirement (4).

beam wall interactions far from the origin; all have $z_{\rm int} < -100$ cm and have showering in the vertex and jet chamber. Three events show evidence of several low angle tracks in the vertex and jet chambers, and two others have small showers only in the vertex chamber. These five events have photons consistent with originating from the interaction point, with $z_{\rm int} > -100$ cm. Hence, they may be from beam gas or beam wall interactions near the origin, although one or more could be the result of general beam backgrounds, as there is an expected loss of 1.5 events as deduced from random triggers. One additional event of this type is observed; it arises from a single electron which undergoes a strong bremsstrahlung in the outer wall of the vertex chamber. The beam wall - beam gas candidates show no dependence on the centre-of-mass energy, and only two of these deposit more than 1.5 GeV in the electromagnetic calorimeter.

Since no material is present to absorb a 1 GeV photon coming from an interaction within 200 cm of the origin, beam gas and beam wall interactions occurring anywhere in this region can contribute background. Two single photon candidates have $z_{\rm int} < -100$ cm,

whereas from the distribution of the single electron candidates we would expect 0.5 such events. In one of the two events, more than 1.5 GeV is deposited in the calorimeter. Assuming a uniform population along the beam axis for beam wall and beam gas events which satisfy the single photon selection, we estimate the contamination of such events in the sample of single photons above 1 GeV to be $2 \pm 2$ events.

The requirement that the coordinates of a presampler cluster match well with the electromagnetic cluster strongly suppresses background from many sources. There is an observed excess of events in figure 5, outside the selected region, with separations between 50 and 200 mrad. Of these 41 events only two have a TOF signal within 2 ns of the expected flight time for a photon coming from the origin, and 20 have no TOF signal at all. A visual inspection finds the two events to be consistent with signal events. The expectation from the $e^+e^- \rightarrow \nu\bar{\nu}\gamma$ Monte Carlo sample is that $1.8 \pm 0.4$ events would populate this region, consistent with the two observed events.

### Electromagnetic calorimeter energy scale and resolution

For a precise measurement of the single photon cross section, at centre-of-mass energies near the $Z^0$ mass, it is essential to understand the scale of the photon energy measurement, since the photon spectrum is a rapidly falling distribution. The single electron sample can be used to study the simulation of energy loss in the coil, and the energy scale and resolution of the calorimeter, because the electron momentum is also well measured from its curvature in the central detector.

The difference between the central detector momentum and the calorimeter energy is shown in figure 9 as a function of momentum and polar angle for data and Monte Carlo single electrons. It is seen that the calorimeter energy scale and mean energy loss in the coil are well simulated The agreement is better than 50 MeV for all energies below 3 GeV and over the full range of polar angle considered. The energy resolution is slightly better in the detector simulation by 20–40 MeV.

This study shows that the detector simulation of the photon energy measurement can be used directly. The energy scale uncertainty at 1.5 GeV is assumed to be 30 MeV, which corresponds to an uncertainty in the single photon acceptance of 2.1 % for the single photon sample above 1.5 GeV. The slight discrepancy in the observed resolutions has a negligible effect on the single photon acceptance.

The selection of single photon events used to determine the $Z^0$ invisible width requires the photons to deposit more than 1.5 GeV in the electromagnetic calorimeter. In order to present total cross sections for single photon events in which the true photon energies are above 1.5 GeV, it is necessary to correct for the energy loss in the coil. A correction coefficient is determined from the Monte Carlo data at each centre-of-mass energy point,

$$C(E_{\rm cm}) = \frac{N(E_{\rm deposit} > 1.5 \text{ GeV}, E_{\rm cm})}{N(E_{\rm true} > 1.5 \text{ GeV}, E_{\rm cm})} \tag{4}$$

where $N$ refers to the number of events passing the single photon selection with the energy cut replaced by the one indicated. Table 2 lists the correction factors thus determined. By

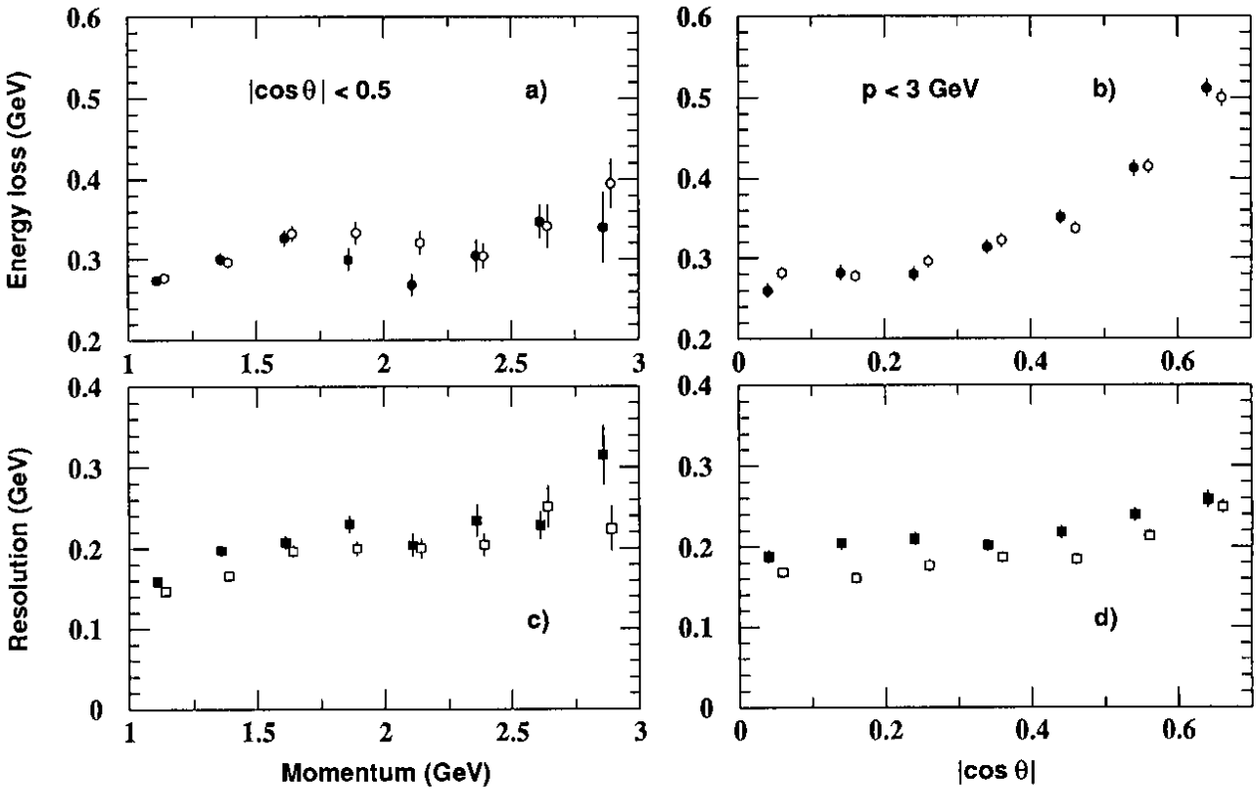


**Figure 9.** The difference in the electron energy measurement by the central detector and by the electromagnetic calorimeter is shown by the circular points as a function of a) the momentum and b) the cosine of the polar angle, for the data (solid circles) and the Monte Carlo (open circles). The resolution of the energy measurement is shown in c) and d). In order to separate the effects of incident momentum and angle, in a) and c) only events with $|\cos\theta| < 0.5$ are considered and in b) and d) only events with $p < 3$ GeV are used.

**Table 2.** The energy correction coefficients listed are the ratios of Monte Carlo single photon events which deposit more than 1.5 GeV in the calorimeter to those whose true energy is above 1.5 GeV. The errors shown are from Monte Carlo statistics; there is in addition a correlated uncertainty of 0.02 from the energy scale uncertainty of 30 MeV.

| $E_{\rm cm}$ (GeV) | $C(E_{\rm cm})$ |
|---|---|
| 88.22 | $0.886 \pm 0.054$ |
| 89.22 | $0.860 \pm 0.049$ |
| 90.22 | $0.829 \pm 0.045$ |
| 91.22 | $0.672 \pm 0.043$ |
| 92.22 | $0.773 \pm 0.029$ |
| 93.22 | $0.826 \pm 0.020$ |
| 94.22 | $0.837 \pm 0.018$ |

varying the calorimeter energy scale and resolution by 30 MeV, this leads to a correlated uncertainty of 0.02 in these coefficients.

**Table 3.** The luminosity and the number of single photon candidates which deposit between 1.0 and 1.5 GeV and more than 1.5 GeV in the calorimeter at each centre-of-mass energy point.

| $E_{\rm cm}$ (GeV) | $\mathcal{L}$ (pb$^{-1}$) | $E < 1.5$ GeV | $E > 1.5$ GeV |
|---|---|---|---|
| 88.22 | 0.400 | 5 | 2 |
| 89.22 | 0.546 | 3 | 2 |
| 90.22 | 0.264 | 2 | 2 |
| 91.22 | 2.752 | 26 | 20 |
| 92.22 | 0.379 | 5 | 5 |
| 93.22 | 0.498 | 11 | 17 |
| 94.22 | 0.473 | 11 | 25 |

## Results

A total of 73 single photon candidates depositing more than 1.5 GeV in the calorimeter is observed in the data sample of 5.3 pb$^{-1}$ used in this analysis. Table 3 shows the luminosity and the number of single photon candidates recorded at each of the seven centre-of-mass energy points.

Efficiency corrections are summarised in table 4 along with the background estimates. For photons depositing more than 1.5 GeV in the calorimeter, the overall efficiency is $72.0 \pm 3.4$ %, and the total number of background events in the sample is estimated to be $8 \pm 2$. The backgrounds do not depend strongly on the centre-of-mass energy. An additional 1.6 % systematic error arises from the uncertainty in the luminosity measurement.[3]

The single photon spectra of deposited energies at each of the centre-of-mass energies are shown in figure 10 along with the Monte Carlo expectations for the process $e^+e^- \rightarrow \nu\bar{\nu}\gamma$, assuming three generations of light neutrinos, and with the backgrounds from the sources discussed above. The Monte Carlo data are corrected to represent the expected number of events. The angular distributions are shown in figure 11 for deposited energies below and above 1.5 GeV. In general, good agreement is observed.

The corrected cross sections are shown in table 5 for the process $e^+e^- \rightarrow \nu\bar{\nu}\gamma$, where a photon is above 1.5 GeV in the angular region $|\cos\theta| < 0.7$ and with no restrictions placed against additional photons. These are determined by using the number of observed events and the integrated luminosity as shown in table 3, applying the efficiency and background corrections given in table 4, and then scaling the results by the coefficients in table 2 to account for the energy loss. Finally, a correction of $+2 \pm 1$ % is applied to account for the restriction against a second photon depositing more than 300 MeV in the electromagnetic calorimeter. The overall systematic error from the uncertainties in these corrections and in the integrated luminosity is 5.6 %. In addition, there is an uncertainty in the corrected cross sections of 0.8 pb from the uncertainty of the background.

An analytical program[19,7] which evaluates the cross section for $e^+e^- \rightarrow \nu\bar{\nu}\gamma$ is used to determine the $Z^0$ invisible width. This program uses an improved Born approximation of equation (1) with an $s$-dependent $Z^0$ width to account for the weak radiative corrections, and uses the method of structure functions to include the higher order electromagnetic radiative corrections. The "reduced" cross section, equation (2), can be rewritten in terms

**Table 4.** Summary of the efficiency of the single photon selection and the background estimates, separated for the samples below and above 1.5 GeV in deposited energy. The occupancy vetos refer to the occupancy requirements in the electromagnetic calorimeter, the vertex and jet chambers, the forward calorimeters, and the hadron calorimeter and muon detectors, from criteria (2), (4), (5), and (7). The backgrounds are quoted as the number of events expected to contribute to the observed single photon sample.

| Efficiencies (%) | $1 < E < 1.5$ GeV | $E > 1.5$ GeV |
|---|---|---|
| trigger | $89.2 \pm 3.1$ | $98.7 \pm 0.1$ |
| occupancy vetos | $97.5 \pm 0.1$ | $97.5 \pm 0.1$ |
| no conversion in central detector | $94 \pm 2$ | $94 \pm 2$ |
| conversion in coil | $82 \pm 3$ | $82 \pm 3$ |
| presampler match | $97 \pm 2$ | $97 \pm 2$ |
| total efficiency (%) | $65.0 \pm 3.8$ | $72.0 \pm 3.4$ |
| **Backgrounds (events)** | | |
| $e^+e^- \to e^+e^-\gamma$ | $13 \pm 2$ | $5 \pm 1$ |
| $e^+e^- \to \gamma\gamma\gamma$ | $1 \pm 1$ | – |
| $e^+e^- \to e^+e^-X$ $(X = f_2, \pi^0, \eta, \eta')$ | $6 \pm 2$ | $1 \pm 1$ |
| $e^+e^- \to e^+e^-l^+l^-\gamma$ | $4 \pm 4$ | – |
| $e^+e^- \to \mu^+\mu^-\gamma$ | $1 \pm 1$ | $1 \pm 1$ |
| beam gas and beam wall interactions | $1 \pm 1$ | $1 \pm 1$ |
| total background (events) | $26 \pm 5$ | $8 \pm 2$ |

of the $Z^0$ invisible width as

$$\sigma_0(s) = \frac{12\pi}{M_Z^2} \frac{s\,\Gamma_e\Gamma_{\rm inv}}{(s - M_Z^2)^2 + s^2\Gamma_Z^2/M_Z^2} + W \text{ terms.} \tag{5}$$

Hence the $Z^0$ invisible width can be specified in the analytical program by $\Gamma_{\rm inv} = N_\nu\Gamma_\nu$, where $N_\nu$ is an arbitrary real number of neutrino generations and $\Gamma_\nu$ is the Standard Model $Z^0$ partial width for each neutrino generation. To describe the $Z^0$ resonance we use as input parameters our most recent measurements[3] of the $Z^0$ mass, $M_Z = 91.17 \pm 0.02$ GeV, and its width, $\Gamma_Z = 2.51 \pm 0.02$ GeV. To define the $Z^0$ partial widths to electrons and neutrinos, we use our measured value, $\sin^2\bar{\theta}_w = 0.232 \pm 0.003$. We allow the real parameter $N_\nu$ to vary, while keeping the total width fixed, to determine the invisible width which corresponds to our observed 73 events. In this determination of the $Z^0$ invisible width we assume that the W contribution is indeed given by the Standard Model, and that no other diagrams, other than those shown in figure 1, lead to final states with a single photon and no other visible particles.

This analysis gives a $Z^0$ invisible width of $0.50 \pm 0.07 \pm 0.03$ GeV. Assuming the Standard Model $Z^0$ coupling to neutrinos, this corresponds to $3.0 \pm 0.4 \pm 0.2$ light neutrino generations. The corrected cross section is shown as a function of centre-of-mass energy in figure 12, along with the expectations for $N_\nu = 2, 3, 4$. As a check of the normalisation

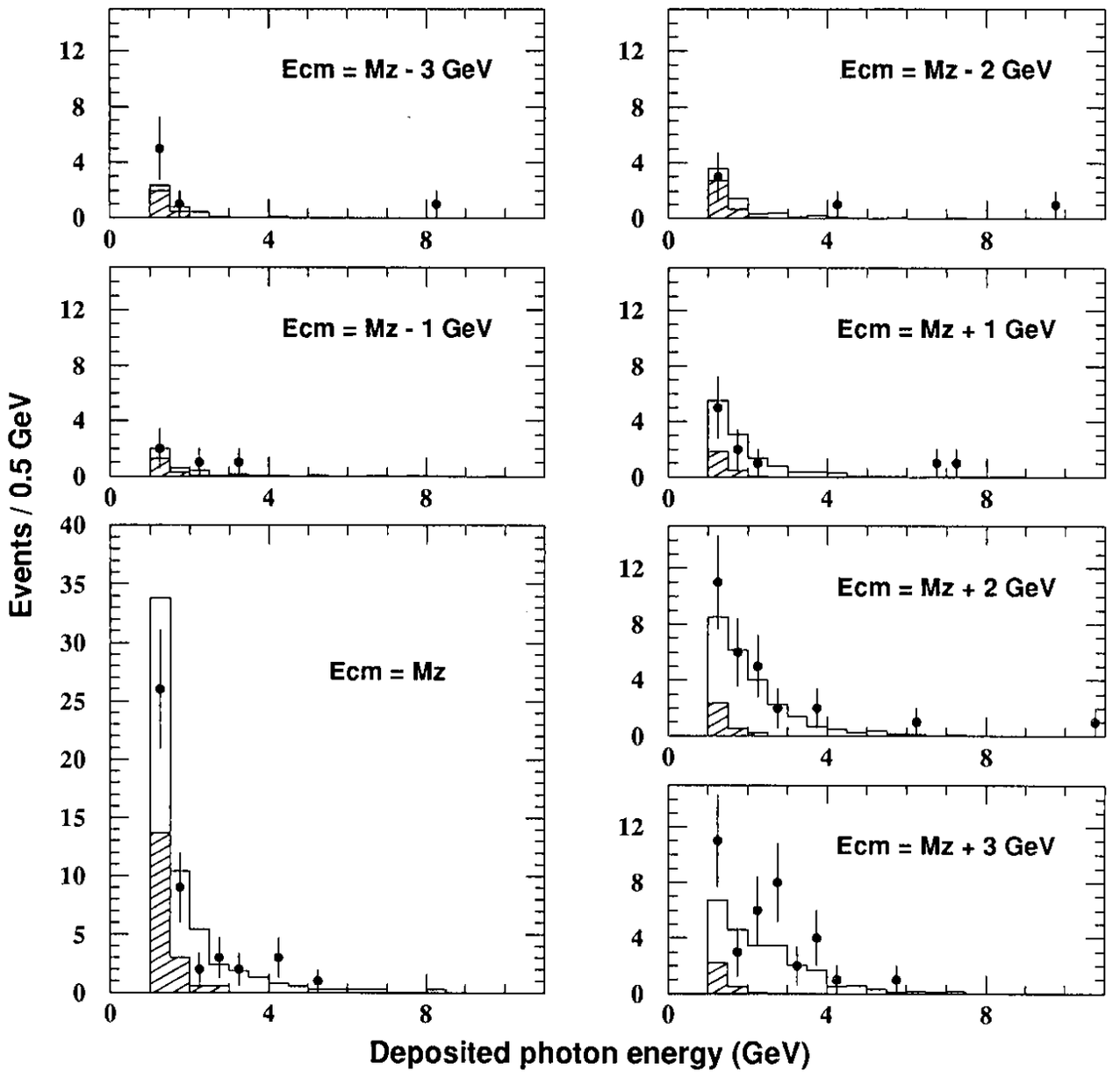


**Figure 10.** The energies deposited in the electromagnetic calorimeter by all the single photon candidates are shown at each of the seven centre-of-mass energy points. Also shown are Monte Carlo expectations, normalised to the recorded luminosities and corrected for trigger and selection efficiencies. The unshaded region of the histogram shows the prediction for the process $e^+e^- \to \nu\bar{\nu}\gamma$ assuming three generations of light neutrinos while the shaded portion corresponds to the component from background. The first bin (between 1 and 1.5 GeV) is not used in the determination of the $Z^0$ invisible width.

of the analytical formula, the Standard Model Monte Carlo $e^+e^- \to \nu\bar{\nu}\gamma$ event generator program[15] is used. The expected number of events is calculated for two, three, and four generations, where in this case the $Z^0$ total width varies with the number of neutrino generations. By interpolation, the value which corresponds to the 73 observed events is $N_\nu = 3.1$.

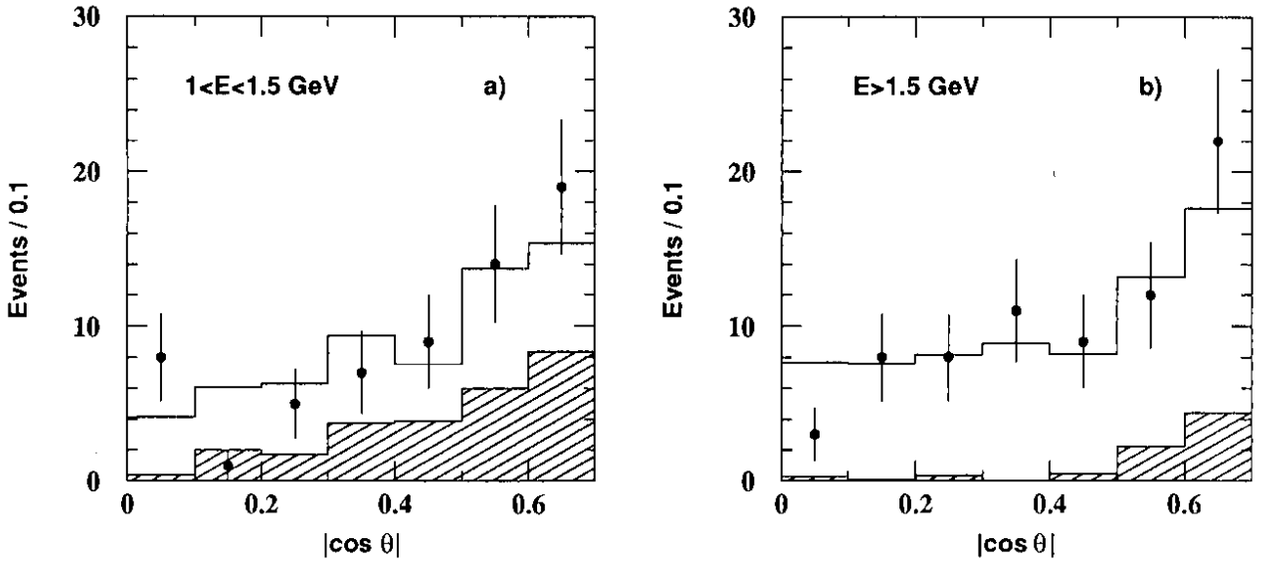


**Figure 11.** The angular distribution for the single photon candidates depositing a) between 1 and 1.5 GeV, b) more than 1.5 GeV in the electromagnetic calorimeter, from the complete data set. Also shown are Monte Carlo expectations, corrected for trigger and selection efficiencies, for the process $e^+e^- \rightarrow \nu\bar{\nu}\gamma$, assuming three generations of light neutrinos (unshaded areas), and the background sources (shaded histograms).

**Table 5.** The corrected cross sections, $\sigma$, are listed at each centre-of-mass energy for single photon production above 1.5 GeV in the angular region $|\cos\theta| < 0.7$ and with no restrictions against additional photons. The errors indicate the uncorrelated uncertainties only. In addition, there are correlated uncertainties of 5.6 % and 0.8 pb.

| $E_{\rm cm}$ (GeV) | $\sigma$ (pb) |
|---|---|
| 88.22 | $6 \pm 6$ |
| 89.22 | $4 \pm 4$ |
| 90.22 | $10 \pm 9$ |
| 91.22 | $12 \pm 4$ |
| 92.22 | $21 \pm 11$ |
| 93.22 | $56 \pm 14$ |
| 94.22 | $87 \pm 18$ |

With this measurement of the invisible width, the number of single photon candidates which deposit between 1 and 1.5 GeV in the electromagnetic calorimeter is expected to be $64 \pm 6$ including backgrounds, in good agreement with the 63 observed events. By using these lowest energy events as a background control sample, the statistical significance of the complete single photon sample is reduced. However, this control sample provides an important check of the background calculations using the data themselves.

## Summary

A direct determination of the $Z^0$ invisible width is performed by measuring the single photon cross section at centre-of-mass energies near the $Z^0$ resonance with the OPAL

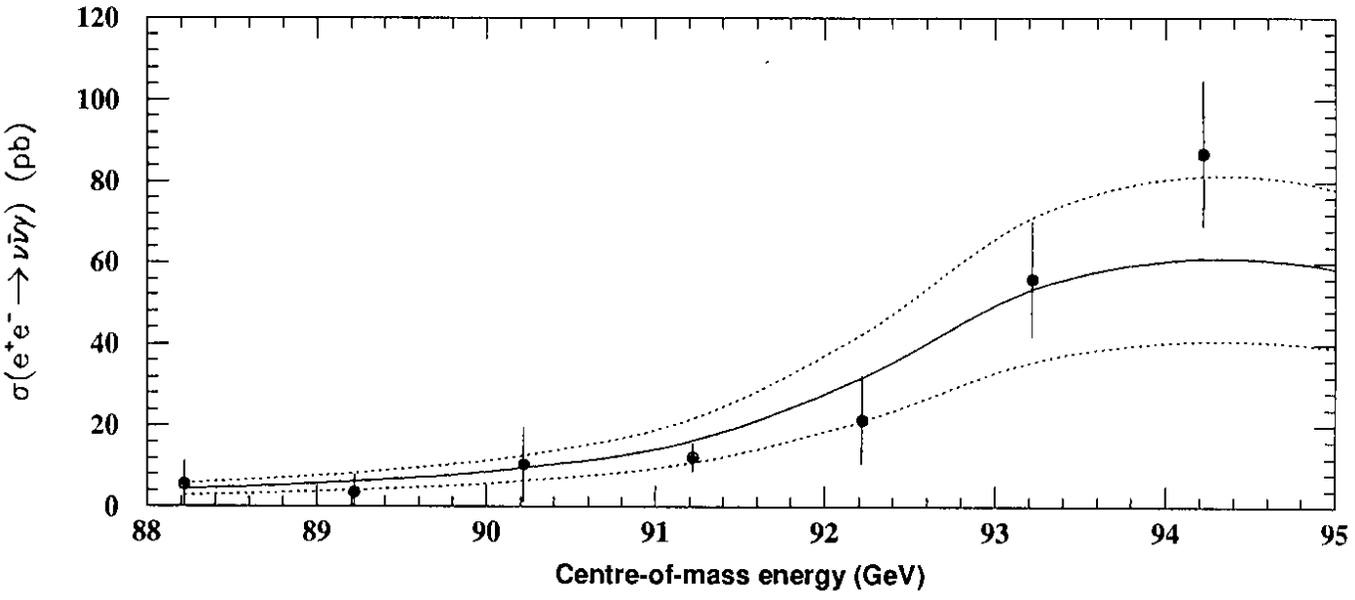


**Figure 12.** The corrected cross sections (pb) at each centre-of-mass energy point for single photons above 1.5 GeV in the angular range $|\cos\theta| < 0.7$ from the process $e^+e^- \to \nu\bar{\nu}\gamma$. The solid curve shows the result corresponding to 3.0 light neutrino generations. The expectations from two and four light neutrino generations are shown by the lower and upper dashed curves respectively.

detector. A total of 136 events are observed in which the photon deposits more than 1 GeV in the electromagnetic calorimeter. The 73 events which deposit more than 1.5 GeV are used to determine the invisible width, $\Gamma_{\rm inv} = 0.50 \pm 0.07 \pm 0.03$ GeV. Assuming the Standard Model $Z^0$ coupling to neutrinos, this corresponds to $3.0 \pm 0.4 \pm 0.2$ light neutrino generations.

## Acknowledgements

It is a pleasure to thank the SL Division for the efficient operation of the LEP accelerator and for its continuing close cooperation with our experimental group. In addition to the support staff at our own institutions we are pleased to acknowledge the following :
The Natural Sciences and Engineering Research Council, Canada.
The Department of Energy, USA.
The National Science Foundation, USA.
The Science and Engineering Research Council, UK.
The Israeli Ministry of Science.
The Minerva Gesellschaft.
The Japanese Ministry of Education, Science and Culture (the Monbusho) and a grant under the Monbusho International Science Research Program.
The American Israeli Bi-national Science Foundation.
The Direction des Sciences de la Matière du Commissariat à l'Energie Atomique, France.
The Bundesministerium für Forschung und Technologie, FRG.
The A. P. Sloan Foundation.

## REFERENCES


1. S. Weinberg, Phys. Rev. Lett. 19 (1967) 1264;
   A. Salam, *Elementary Particle Theory*, ed. N. Svartholm (Almquist and Wiksells, Stockholm, 1969) p.367;
   S. L. Glashow, J. Iliopoulos and L. Maiani, Phys. Rev. D2 (1970) 1285.
2. D. Yu. Bardin *et al.*, Berlin-Zeuthen preprint PHE 89-19, 1989.
3. OPAL collaboration, contribution by T. Mori to 25th International Conference on High Energy Physics, Singapore, August 1990;
   OPAL collaboration, M. Z. Akrawy *et al.*, Phys. Lett. B240 (1990) 497.
4. C. Jarlskog, Phys. Lett. B241 (1990) 579.
5. ALEPH collaboration, D. Decamp *et al.*, Zeit. Phys. C48 (1990) 365;
   DELPHI collaboration, P. Abreu *et al.*, contribution to 25th International Conference on High Energy Physics, Singapore, CERN-PPE/90-119, August 1990;
   L3 collaboration, B. Adeva *et al.*, Phys. Lett. B249 (1990) 341.
6. A. D. Dolgov, L. B. Okun and V. I. Zakharov, Nucl. Phys. B41 (1972) 197;
   E. Ma and J. Okada, Phys. Rev. Lett. 41 (1978) 287;
   K. J. F. Gaemers, R. Gastmans and F. M. Renard, Phys. Rev. D19 (1979) 1605;
   G. Barbiellini, B. Richter and J. L. Siegrist, Phys. Lett. 106B (1981) 414.
7. L. Trentadue *et al.* in *Z Physics at LEP1*, G. Altarelli ed., CERN 89-08 (1989) 129.
8. MAC collaboration, W. T. Ford *et al.*, Phys. Rev. D33 (1986) 3472;
   H. Wu, Ph.D. Thesis (unpublished) Universität Hamburg, 1986;
   CELLO collaboration, H.-J. Behrend *et al.*, Phys. Lett. 215B (1988) 186;
   ASP collaboration, C. Hearty *et al.*, Phys. Rev. D39 (1989) 3207.
9. VENUS collaboration, K. Abe *et al.*, Phys. Lett. 232B (1989) 431.
10. OPAL collaboration, K. Ahmet *et al.*, submitted to Nucl. Instr. and Meth., CERN-PPE/90-114, August 1990.
11. J. Allison *et al.*, Comp. Phys. Comm. 47 (1987) 55;
    R. Brun *et al.*, GEANT 3, Report DD/EE/84-1, CERN (1989).
12. D. Karlen, Nucl. Phys. B289 (1987) 23.
13. R. Battacharya, J. Smith and G. Grammer, Phys. Rev. D15 (1977) 3267;
    J. Smith, J. A. M. Vermaseren and G. Grammer, Phys. Rev. D15 (1977) 3280.
14. OPAL collaboration, M. Z. Akrawy *et al.*, Phys. Lett. B241 (1990) 133.
15. R. Miquel, C. Mana and M. Martinez, Zeit. Phys. C48 (1990) 309;
    F. A. Berends, G. Burgers, C. Mana, M. Martinez and W. L. van Neerven, Nucl. Phys. B301 (1988) 583.
16. F. A. Berends and R. Kleiss, Nucl. Phys. B186 (1981) 22.
17. W.G.J. Langeveld, Ph.D. Thesis (unpublished) Rijksuniversiteit Utrecht, 1986.
18. S. Jadach, B.F.L. Ward, Z. Was, R.G.S. Stuart and W. Hollik, to be published in Comp. Phys. Comm.;
    T. Sjöstrand and M. Bengtsson, Comp. Phys. Comm. 43 (1987) 367;
    G. Marchesini and B. R. Webber, Nucl. Phys. B310 (1988) 461.
19. O. Nicrosini and L. Trentadue, Nucl. Phys. B318 (1989) 1.




Imprimé au CERN. Prix : 0.80 Fr.